

1 Environmental chemical diethylhexyl phthalate alters intestinal microbiota community structure
2 and metabolite profile in mice

3

4 Ming Lei^{a,1}, Rani Menon^{b,1}, Sara Manteiga^{a,†}, Nicholas Alden^a, Carrie Hunt^d, Robert C. Alaniz^d,
5 Kyongbum Lee^{a,*,#}, and Arul Jayaraman^{b,c,d,*}

6

7 ^a. Department of Chemical and Biological Engineering, Tufts University, Medford, MA 02155

8 ^b. Artie McFerrin Department of Chemical Engineering, Texas A&M University, College Station,
9 Texas 77843

10 ^c. Department of Biomedical Engineering, Texas A&M University, College Station, TX 77843

11 ^d. Department of Microbial Pathogenesis and Immunology, College of Medicine, Texas Health
12 Science Center, Texas A&M University, College Station, TX 77843

13 ^e. Artie McFerrin Department of Chemical Engineering, Texas A&M University, College
14 Station, TX 77843

15

16 Running Head: Phthlate-induced microbiota alterations in mice

17

18 ¹: M.L. and R.M. contributed equally to the work

19 [†]: Present address: Sara Manteiga, 50 Northern Ave, Boston, MA 02210

20 ^{*}: Corresponding authors: Kyongbum Lee and Arul Jayaraman

21 [#]: Lead contact: Kyongbum Lee, kyongbum.lee@tufts.edu

22 **Abstract**

23 Exposure to environmental chemicals during windows of development is a potentially
24 contributing factor in gut microbiota dysbiosis, and linked to chronic diseases and developmental
25 disorders. We used a community-level model of microbiota metabolism to investigate the effects
26 of diethylhexyl phthalate (DEHP), a ubiquitous plasticizer implicated in neurodevelopmental
27 disorders, on the composition and metabolite outputs of gut microbiota in young mice.
28 Administration of DEHP by oral gavage increased the abundance of *Lachnospirillum*, while
29 decreasing *Akkermansia*, *Odoribacter*, and *Clostridium sensu stricto*. Addition of DEHP to *in*
30 *vitro* cultured cecal microbiota increased the abundance of *Alistipes*, *Paenibacillus*, and
31 *Lachnospirillum*. Untargeted metabolomics showed that DEHP broadly altered the metabolite
32 profile in the culture. Notably, DEHP enhanced the production of *p*-cresol, while inhibiting
33 butyrate synthesis. Metabolic model-guided correlation analysis indicated that the likely sources
34 of *p*-cresol are *Clostridium* species. Our results suggest that DEHP can directly modify the
35 microbiota to affect production of bacterial metabolites linked with neurodevelopmental
36 disorders.

37 **Importance**

38 Several previous studies have pointed to environmental chemical exposure during windows of
39 development as a contributing factor in neurodevelopmental disorders, and correlated these
40 disorders with microbiota dysbiosis, little is known about how the chemicals specifically alter the
41 microbiota to interfere with development. The findings reported in this paper unambiguously
42 establish that a pollutant linked with neurodevelopmental disorders can directly modify the
43 microbiota to promote the production of a potentially toxic metabolite (*p*-cresol) that has also
44 been correlated with neurodevelopmental disorders. Further, we use a novel modeling strategy to
45 identify the responsible enzymes and bacterial sources of this metabolite. To the best of our

46 knowledge, the present study is the first to characterize the functional consequence of phthalate
47 exposure on a developed microbiota. Our results suggest that specific bacterial pathways could
48 be developed as diagnostic and therapeutic targets against health risks posed by ingestion of
49 environmental chemicals.

50

51

52

53

54 **Introduction**

55 The mammalian gastrointestinal (GI) tract harbors microbial communities that impact a wide
56 array of physiological functions, including digestion, immune system development, and defense
57 against pathogens. Alterations in the microbiota composition leading to functional imbalance, or
58 dysbiosis, have been linked to various chronic diseases and disorders, including inflammatory
59 bowel disease (1), colorectal cancer (2), fatty liver disease (3), diabetes (4), and
60 neurodevelopmental disorders (5). Factors known to cause dysbiosis include diet, infection, and
61 use of antibiotics. In recent years, environmental chemicals have emerged as another factor
62 contributing to alterations in the microbiota.

63 Exposure to biologically active synthetic chemicals present in household and industrial
64 products, particularly during critical windows of development, has been shown to result in
65 microbiota dysbiosis and correlated to various disorders of the immune and nervous systems (6).
66 An environmental chemical that is pervasive in the environment due to its widespread use as a
67 plasticizer is diethylhexyl phthalate (DEHP) (7). In vertebrate animals, DEHP impacts
68 reproduction and development (8). A recent study found increased serum DEHP concentrations
69 in children diagnosed with autism spectrum disorder (ASD) (9). Additionally, fecal samples from

70 children diagnosed with ASD have elevated concentrations of bacterial metabolites such as *p*-
71 cresol (10), pointing to a potential link between the health effects of DEHP exposure and the
72 intestinal microbiota.

73 This link is supported by multiple studies with other environmental chemicals correlating
74 microbiota dysbiosis with adverse effects of exposure. A study in mice showed that exposure to
75 benzo[a]pyrene resulted in pronounced alterations of the intestinal microbiota, including a
76 decrease in the abundance of *Akkermansia muciniphila*, and an increase in the levels of
77 inflammatory indicators (11). Another recent study found that Bisphenol-A (BPA) exposure
78 exacerbated the effects of chemically-induced colitis, and that these effects were accompanied by
79 altered fecal levels of tryptophan-derived metabolites (12).

80 The importance of bacterially produced metabolites in dysbiosis-related disorders was
81 highlighted by Hsiao et al., who showed that the behavioral abnormalities observed in a
82 maternal immune activation (MIA) model of anxiety-like behavior in mice correlated with
83 changes in the abundance of intestinal bacteria and the concentration of bacterial metabolites in
84 serum (13). This study also showed that the behavioral abnormalities in the MIA model could be
85 improved by controlling the level of a specific tyrosine metabolite, 4-ethylphenylsulfate. Altered
86 levels of microbiota-associated metabolites such as indoxyl sulfate and *p*-hydroxyphenyllactate
87 have also been detected in blood and urine of children diagnosed with ASD (14, 15), suggesting
88 that the link between bacterial metabolites and neurodevelopmental disorders could be relevant
89 in humans. On the other hand, it is unclear whether the aforementioned alterations in bacterial
90 metabolite profiles directly result from environmental chemical exposure. While several studies
91 have investigated the effects of DEHP exposure on host reproductive, nervous and metabolic
92 tissues (16-18), little is known about the impact of this ubiquitous chemical on intestinal
93 microbiota composition and function.

94 A majority of studies have used early life exposure models to study the effects of
95 environmental chemicals on the intestinal microbiota. Observations from these studies suggest
96 that changes to the intestinal microbiota can persist beyond the pre- or perinatal exposure period
97 (19, 20). For example, perinatal exposure of rabbits to BPA *in utero* and during the first week of
98 nursing led to a decrease in short-chain fatty acid (SCFA) producing bacteria at 6 weeks of age
99 (21). Another study found that continuous exposure to diethyl phthalate, methylparaben, and
100 triclosan beginning at birth induced significant changes to the gut microbiota of adolescent rats
101 (22). To-date, few studies have looked at the effect of environmental chemical exposure on a
102 developed microbiota.

103 While *in vivo* studies on the microbiota offer physiologically relevant insights, they can
104 be often difficult to interpret due to confounding influences from the host (23). Apart from
105 directly altering microbiota composition, environmental chemicals can also indirectly cause
106 microbiota dysbiosis, for example by bringing about intestinal inflammation through activation
107 of host receptors (24). Moreover, receptor activation can occur through an intestinal or liver
108 biotransformation product, rather than the chemical itself (25). To elucidate the mechanistic role
109 of dysbiosis resulting from environmental chemical exposure in a particular disease or disorder,
110 it is important to delineate the effects of environmental chemical exposure on the intestinal
111 microbiota from those on the host.

112 In this work, we used *in vivo* exposure in mice and an *in vitro* culture model to
113 investigate the effect of DEHP on the intestinal microbiota composition and its metabolite
114 output. Our results suggest that environmental chemical exposure can directly modify the
115 intestinal microbiota to increase production of potentially neurotoxic microbial metabolites
116 linked with behavioral abnormalities.

117

118 **Results**

119 ***Gut microbiota composition is altered in vivo in a time dependent manner***

120 We investigated the effect of DEHP exposure on the gut microbiota by administering the
121 chemical to 6-8 week old female C57/BL6 mice via oral gavage and analyzing the changes in the
122 fecal microbial community at day 7 and day 14 post-exposure using 16S rRNA sequencing.
123 Principal component analysis (PCA) of operational taxonomic unit (OTU) counts showed
124 samples grouping together by time point but not by DEHP treatment (Figure 1A), suggesting that
125 changes in OTU profile driven by the host's age may dominate over DEHP-driven changes. This
126 trend agreed with classification results from partial least squares-discriminant analysis (PLS-
127 DA), which achieved stronger separation between OTU profiles when samples were classified
128 based on time point than chemical treatment (Figure S1). The results from PLS-DA also
129 indicated that the effect of DEHP on the OTU profiles was greater on day 7 than day 14.
130 Consistent with this observation, samples from DEHP treated mice showed a higher alpha
131 diversity (Chao1 index) than control mice on day 7, but not day 14 (Figure 1B). Similarly, linear
132 discriminant analysis of the effect size (LefSe) identified a larger number of OTUs affected by
133 DEHP treatment in day 7 samples compared to day 14 samples (Figure 1C). At the genus level,
134 the abundance of *Akkermansia*, *Odoribacter*, and *Clostridium sensu stricto* decreased in the
135 DEHP samples collected on day 7. Of these, only *Clostridium sensu stricto* remained
136 significantly depleted in the day 14 samples. An unclassified genus belonging to the order
137 *Mollicutes RF9* was increased in abundance in the DEHP samples on day 7, and
138 *Lachnoclostridium* was increased on day 14.

139

140 ***Fecal metabolite profile is more strongly influenced by host-dependent factors than DEHP***
141 ***treatment***

142 To determine whether the phthalate exposure also altered the profile of intestinal metabolites, we
143 analyzed the fecal material using untargeted LC-MS metabolomics. We first confirmed that the
144 orally administered DEHP was available to the microbiota by identifying the presence of
145 mono(2-ethylhexyl)phthalate (MEHP), a product of enzyme-catalyzed DEHP degradation (26) in
146 the metabolite data. As expected, MEHP was detected in fecal samples from DEHP treated mice,
147 but not control mice (Figure 2A). Similar to the OTU profiles, results of PCA on the LC-MS
148 features indicated that DEHP had a lesser effect on the fecal metabolite profile than the host's
149 age (Figure 2B). This result was consistent with two-tailed t-tests performed on individual data
150 features, i.e., metabolites, which found very few statistically significant differences (none that
151 could be assigned a putative identity) between time-matched samples from control and DEHP-
152 treated mice on days 0, 7, and 14 (less than 1.6, 2.3, and 8.0% of total detected features,
153 respectively). We detected a larger number of features that were significantly elevated or reduced
154 in the day 14 fecal samples relative to day 0 and 7 samples (10.9 and 23.7%, respectively). These
155 trends suggested that the global profile of fecal metabolites is more strongly influenced by host
156 factors such as aging. To more directly assess the effects of DEHP on the microbiota in isolation
157 from host influences, we performed the DEHP exposure experiment using an anaerobic batch
158 culture model of murine cecal microbiota.

159

160 *Anaerobic cecal batch culture captures in vivo microbiota diversity*

161 We assessed whether the cecal contents culture could represent the biochemical diversity of
162 murine cecal microbiota by characterizing the OTU profile of control cultures in gut microbiota
163 medium (GMM) (27) without DEHP. Using QIIME with the SILVA database (28) as the
164 reference, we identified approximately 2,000 distinct OTUs that are present on both days 1 and 7
165 of the culture. Nearly all of the OTUs (99.4 %) belong to four bacterial phyla: *Actinobacteria*,

166 *Bacteroidetes*, *Firmicutes*, and *Proteobacteria* (Figure 3A). The number of families and genera
167 represented in the culture were 65 and 119, respectively. A comparison of OTUs detected on day
168 7 of cultured cecal contents with cecal contents harvested from 8-week old female C56/BL6
169 mice showed 100% similarity in relative abundance at the phylum level and greater than 70%
170 similarity at the genus and species levels (Figure S2). From day 1 to 7, there were significant
171 shifts in the relative abundances of the OTUs. At the genus level, *Lactobacillus* and
172 *Parabacteroides*, respectively, showed the maximum decrease and increase in terms of OTU
173 counts, whereas *Fluviicola* and *Enterococcus*, respectively, showed the greatest decrease and
174 increase in terms of fold-change (Figure 3B).

175

176 ***Cecal culture produces a diverse array of secondary and amino acid metabolites***

177 We next characterized the major metabolic products and substrates of the cecal cultures using
178 untargeted LC-MS experiments. Principal component analysis (PCA) performed on the
179 untargeted LC-MS features showed clear separation between day 1 and 7 samples from the
180 inoculated GMM cultures (Figure 4A). In contrast, day 1 and 7 samples from culture tubes
181 containing GMM without cells grouped closely together. Hierarchical clustering of the LC-MS
182 data features revealed five distinct patterns (Figure 4B). The first group of features represented
183 metabolites that were rapidly consumed and significantly depleted by day 1. A second, larger
184 group was consumed more slowly, with significant depletion occurring only by day 7. The third
185 group comprised rapidly produced metabolites that were significantly elevated by day 1. The
186 fourth group of metabolites was produced more slowly, and significantly elevated by day 7, but
187 not day 1. The fifth group was significantly elevated by day 1, but reduced by day 7 (Figure 4C).

188 Putative metabolite identities were assigned to the LC-MS data features based on
189 accurate mass and product ion spectra (MS/MS data). Overall, 118 and 156 of the features in the

190 positive and negative mode ionization data, respectively, were assigned a putative KEGG
191 compound identifier. The merged list of putatively identified metabolites from both ionization
192 modes comprised 204 unique compounds (Table S1). The overlap in metabolites identified by
193 positive and negative mode experiments was very small (27/231), indicating that using two
194 different LC-MS methods significantly broadened coverage.

195 We utilized the Search Pathway tool of KEGG Mapper to associate each putatively
196 identified metabolite with one or more functional categories (Table S2). Based on this mapping,
197 the largest KEGG function categories were biosynthesis of secondary metabolites (54 mapped
198 metabolites), microbial metabolism in diverse environments (47), and biosynthesis of antibiotics
199 (35). Additional pathways captured by the data included fermentative reactions known to occur
200 in the intestine, such as L-carnitine metabolism to gamma-butyrobetaine and trimethylamine. If
201 the different amino acid metabolism subcategories were pooled, then more than one-third
202 (79/204) of the metabolites belonged to this more general category. Interestingly, we detected the
203 production of the neurotransmitter serotonin, despite the absence of any host cells in the cultures.
204 Other aromatic amino acid (AAA) products including the tryptophan metabolites indole (Figure
205 4D), indole-3-propionic acid and indole-3-carboxylic acid were also detected. Phenylalanine-
206 derived metabolites detected in the cultures included phenylacetic acid, phenylpropionic acid,
207 and 3-(3-hydroxyphenyl)propionic acid, and tyrosine-derived metabolites detected included *p*-
208 cresol and *p*-hydroxyphenylacetic acid.

209

210 ***Metabolic function in cecal cultures is distributed heterogeneously across taxonomic groups***

211 We next analyzed the genomes of bacterial groups detected in the culture to characterize the
212 enzymatic reactions responsible for the metabolic products. Cross-referencing the list of
213 identified OTUs against KEGG and UniProt, we obtained a model that included at least one

214 annotated genome for 94 of 119 genera detected in the cultures, accounting for greater than 96%
215 of the bacterial counts (Figure 5A).

216 We evaluated the coverage of metabolic functions represented in the model by comparing
217 the orthologs of the model against the orthologs predicted by Tax4Fun (29), using 16S sequence
218 data, reference sequences in the SILVA database, and annotated genomes cataloged in KEGG as
219 inputs. Based on KEGG orthology (KO) numbers, 83% of the gene functions predicted by
220 Tax4Fun overlapped with the estimates from our model. When weighted by the relative
221 abundance of the OTUs, we found a strong correlation between ortholog counts from Tax4Fun
222 and our model (Figure S3). Despite the similarity in functional coverage with our model, the
223 Tax4Fun prediction included many additional organisms most of which (more than 80%) did not
224 match the OTUs classified by the SILVA analysis on the cecal culture. Thus, our model
225 parsimoniously covered the biochemical diversity of the cecal culture without overpredicting the
226 underlying taxonomic diversity.

227 The molecular functions represented by KO numbers were used to associate the bacterial
228 species in our model with enzymatic reactions and their corresponding metabolites. The
229 reactions distributed highly unevenly across the different genera (Figure 5B). Out of more than
230 4,000 reactions, only 4 (involved in DNA replication) mapped to every genus. Approximately
231 9% (349/4034) of the reactions mapped to a single genus, indicating that certain metabolic
232 functions (e.g., carotenoid biosynthesis, steroid hormone biosynthesis, methane metabolism,
233 glycosphingolipid biosynthesis, benzoate degradation) required the participation of particular
234 genera. Based on reaction definitions in KEGG, 84% (49/58) of the confidently identified
235 metabolites (Table S3) were mapped to one or more organisms in the model. Similar to the trend
236 for reactions in the model, the metabolites also distributed heterogeneously across the different
237 organisms. Amino acids (e.g., phenylalanine, tryptophan), nucleosides/nucleotides (e.g., uridine,

238 uracil), and vitamins (e.g., riboflavin) associated with nearly ubiquitous reactions found in more
239 than 90% of the genera, whereas certain fermentation products (e.g., benzaldehyde, indole-3-
240 acetate) associated with rare reactions found in less than 50% of the genera.

241

242 ***Correlation analysis finds significant associations between metabolite levels and relative***
243 ***abundance of organisms in the culture***

244 To identify significant associations between individual OTUs and metabolites, we calculated
245 Pearson correlation coefficients (PCCs) between the peak area of each confidently identified
246 metabolite and the relative abundance of each highly abundant genus (>0.05% of total OTU
247 counts) detected on both days 1 and 7. After correcting for false discovery rate (FDR), we found
248 46 significant correlations. We mapped these correlations to the metabolic model described
249 above to highlight different interactions between organisms and metabolites based on whether or
250 not an organism possessed the enzyme to directly act on the correlated metabolite. The resulting
251 correlation network is shown as connected nodes in a bipartite graph (Figure 5C). Excluding
252 common amino acids and GMM components, the strongest correlations were: *Lactobacillus*-
253 lactate (PCC=0.98), *Butyricoccus*-serotonin (PCC=0.93) *Enterococcus*-3-(3-hydroxyphenyl)
254 propionic acid (PCC=0.92), *Clostridium*-indoxyl (PCC=0.91), and *Alistipes*-N1-
255 acetylspermidine (PCC=0.88). (Figure 5C, Table S4).

256

257 ***DEHP induces changes in microbiota composition in vitro***

258 We next examined the effects of DEHP on bacterial abundance in the cecal culture. At the genus
259 level, DEHP increased the abundance of *Alistipes*, *Paenibacillus*, and *Lachnoclostridium* on day
260 1, while decreasing the abundance of *Fluviicola* and *Symbiobacterium*. On day 7, we detected an
261 increase in *Tissierella* (Figure 6A). At the OTU level, DEHP increased *Alistipes putredinis*,

262 *Lachnospiridium bolteae*, and *Lachnospiridium sacharolyticum* on day 1. On day 7, we
263 detected an increase in *Tissierella praecuta*, and decreases in *Bacillus velezensis* and
264 *Lactobacillus brevis*. Overall, DEHP exerted a greater effect on microbiota composition on day 1
265 compared to day 7, both in terms of number of altered OTUs as well as the changes in relative
266 abundance of these OTUs.

267

268 ***DEHP broadly alters metabolite profile of cecal microbiota***

269 Addition of DEHP significantly altered the profile of metabolites in the cultures (Figure 4A). At
270 10 and 100 μM , DEHP altered 16.8% and 20% of the LC-MS features detected on day 7 in the
271 positive ionization mode experiment (Figure S4). The negative mode data showed even greater
272 effects, with 46.7 and 47.2% of the detected features altered at 10 and 100 μM , respectively.
273 Only a subset of these features could be assigned a chemical identity due to lack of matching
274 entries in reference databases. Similar to the in vivo exposure, we detected a dose-dependent
275 accumulation of MEHP, a degradation product of DEHP (Figure S5), confirming that the cecal
276 culture is also capable of this reaction. Figure 4C shows representative profiles of confirmed
277 metabolic products that were increased (cresol) and decreased (butyric acid) by DEHP treatment.
278 *p*-cresol was identified by matching both the m/z ratio and retention time. We observed a
279 retention time shift running the LC method for samples vs pure standards, possibly due to matrix
280 effects of the samples. To account for this shift, we used local linear regression (Figure S6).
281 Additionally, oleic acid and linoleic acid were decreased in the DEHP-treated cultures on day 7,
282 while isatin was increased. An additional feature detected in positive mode ionization at m/z
283 138.0886 had a dose-dependent increase in response to DEHP, and was putatively identified as
284 tyramine, 1-methylnicotinamide, or 2-hydroxyphenethylamine. It was not possible to assign a

285 unique identity, because the product ion spectrum indicated that the corresponding ion
286 chromatogram peak could represent more than one compound.

287

288 **Discussion**

289 Studies have implicated dysbiosis of the gut microbiota in developmental disorders associated
290 with exposure to environmental toxicants (22, 30). In this work, we focus on the effects of
291 DEHP, a pervasive environmental chemical and endocrine disruptor associated with
292 neurodevelopmental disorders such as ASD (9). Previous *in vivo* studies (30, 31) used early-life
293 exposure models to investigate the microbiota's role in developmental health and disease. Fewer
294 studies have investigated the effect of environmental chemical exposure on a developed
295 microbial community in mammals. In the present study, we mimicked human exposure during
296 adolescence by continuously exposing mice to DEHP from ages 6 to 8 weeks. Additionally, we
297 used an anaerobic batch culture model to investigate the effects of DEHP on the microbiota
298 community structure and metabolites.

299 Continuous DEHP exposure modestly increased the alpha-diversity of the fecal
300 microbiota after 7 days, an effect that dissipated by day 14. While it is often assumed that a
301 diverse gut microbiome is beneficial for the host, this is not necessarily the case, as gut health is
302 also impacted by the microbial enterotype. After 14 days, mice exposed to DEHP showed an
303 increased abundance of *Lachnospirillum* and an unclassified genus of *Clostridiales* Family
304 XIII. While the effect of DEHP on gut microbiota of young mice has not been previously
305 reported, studies in humans have associated overrepresentation of *Lachnospirillum* species
306 with neurodevelopmental disorders such as ASD (32, 33). This suggests that the enterotype
307 resulting from pollutant exposure could play a role in dysbiosis associated neurodevelopmental
308 disorders.

309 We detected minimal changes in metabolite profile of fecal material from mice exposed
310 to DEHP for 7 or 14 days. This could be due to several factors. First, host-driven changes, e.g.,
311 due to development and age, could mask subtler effects of phthalate exposure. Second, microbial
312 metabolites can be taken up and transformed by the host, which limits the extent to which fecal
313 metabolite analysis can capture the profile of microbiota metabolites in the intestine. Moreover,
314 fecal metabolites comprise not only bacterial products, but also dietary residues and endogenous
315 metabolites produced by the host. To address these issues, we investigated the effect of DEHP
316 exposure on gut microbiota community structure and biochemical function using an *in vitro*
317 model.

318 *In vitro* models of the intestinal microbiota vary in their complexity, depending on the
319 intestinal location is being mimicked and the degree of biophysical detail being incorporated
320 (34). In the present study, we used a relatively simple anaerobic batch culture model, as the focus
321 was on capturing biochemical function. This model recapitulated up to 70% of the microbiota
322 found in murine cecum at the genus level, including strict anaerobes. Importantly, the culture
323 supported the production of metabolites typically associated with fermentation of sugar and
324 amino acid residues by intestinal bacteria. As the culture system lacks host cells, all of the
325 accumulating products are unequivocally sourced from the detected bacteria. Among the
326 detected products are potentially toxic compounds derived from AAAs, e.g., phenylethylamine
327 (35) and phenylacetic acid (36). We also detected metabolites that are normally present at low
328 levels in the intestine of healthy individuals but are elevated in developmental disorders. For
329 example, 3-phenylpropionic acid and 3-(3-hydroxyphenyl) propionic acid are precursors of 3-(3-
330 hydroxyphenyl)-3 hydroxypropionic acid (HPHPA), a compound elevated in the urine of
331 children diagnosed with ASD (37). Another useful feature of the culture model is that the
332 correlations identified between different metabolites as well as metabolites and organisms can

333 reveal the sources of particular metabolic products. For example, lactic acid accumulated in the
334 culture by day 1 and was rapidly consumed by day 7, which correlated with a significant
335 depletion in *Lactobacillus*, a known lactic acid producer. The depletion in lactic acid was
336 significantly correlated with butyric acid production, consistent with previous reports on
337 bacterial conversion of lactic acid to butyric acid *in vitro* (38). Taken together, these findings
338 suggest that the anaerobic batch culture broadly captures representative metabolic functions of
339 the murine gut microbiota, while facilitating identification of bacterial metabolites and their
340 source organisms.

341 We further analyzed the organism-metabolite correlations using a metabolic model to
342 associate the correlations with enzymatic pathways encoded in the genomes of detected OTUs.
343 Several of these associations confirm previously reported findings. For example, our analysis
344 links *Bacillus* with riboflavin, consistent with previous reports on the synthesis of this vitamin by
345 intestinal *Bacillus* species (39). Likewise, members of the genus *Alistipes* possess the enzyme
346 putrescine N-acetyltransferase (EC# 2.3.1.57), which converts putrescine into N-acetylputrescine
347 (40). A third example is the production of *p*-cresol, which previous reports have attributed to
348 *Clostridium* species (41). Our analysis links *Clostridium* to *p*-hydroxyphenylacetic acid, which is
349 converted to *p*-cresol via *p*-hydroxyphenylacetate decarboxylase (42).

350 Not all of the significant correlations mapped to an enzyme in the metabolic model. One
351 limitation of the model is that genome annotations in KEGG and UniProt are incomplete. For
352 example, the annotations for *Parabacteroides* in the databases did not include an enzyme for
353 butyric acid synthesis, but a recent study found *buk* (butyrate kinase) and *ptb*
354 (phosphotransbutyrylase) in the genomes of intestinal *Parabacteroides* species (43). In this
355 regard, correlations that do not map to a cataloged enzyme could facilitate discovery of
356 previously unknown metabolic functions of intestinal bacteria. Two putatively identified

357 compounds, indoxyl or oxindole and isatin, strongly correlated with the expansion of
358 *Clostridium* and *Parabacteroides*, respectively. Currently known metabolic reactions that
359 produce indoxyl and isatin are catalyzed by monooxygenases requiring oxygen (44). As
360 evidenced by the growth of obligate anaerobes, molecular oxygen is absent in the cultures,
361 suggesting that there could be alternative mechanisms of incorporating hydroxyl groups into
362 metabolites. Indeed, oxindole and isatin have been reported to be products of anaerobic indole
363 degradation (45, 46).

364 Gut microbes have an extensive capacity to break down xenobiotics, including
365 environmental chemicals, which can modulate their toxicity and bioavailability in the host (47).
366 As was the case *in vivo*, we detected a dose-dependent accumulation of MEHP in the cecal
367 contents culture, indicating that the organisms expressing the required esterase are also present *in*
368 *vitro*. Compared to *in vivo* exposure, we detected fewer changes in the microbiota composition
369 upon DEHP addition to the culture medium. This is possibly due to the rapid degradation of
370 DEHP, which was continuously administered to the mice, but added as a bolus at the start of the
371 culture. Nevertheless, we observed features common to both *in vivo* and *in vitro* exposures.
372 Similar to the *in vivo* experiment, we detected an increase in *Lachnoclostridium*, although this
373 increase was transient in the cultures. Additionally, we detected a transient increase in *Alistipes*,
374 which has also been reported for subjects diagnosed with ASD and related GI conditions (48).

375 Treatment with DEHP significantly altered the profile of metabolic products
376 accumulating in the culture. Notably, DEHP increased the accumulation of *p*-cresol, a putative
377 biomarker of ASD (49), while decreasing the levels of butyric acid, a bacterial metabolite
378 benefiting intestinal immune homeostasis and offering neuroprotective effects (50). The likely
379 source of *p*-cresol is tyrosine metabolism by *Clostridium* species (51), although the specific
380 strains responsible remain to be elucidated. We also detected a DEHP-dependent increase in the

381 level of a metabolite putatively identified as isatin. A recent study in rats found that surgical
382 delivery of indole to the cecum leads to isatin and oxindole accumulation in the brain, while
383 decreasing motor activity (52). Taken together, these results suggest that the gut microbiota
384 could be the source of potentially harmful metabolites previous studies have associated with
385 neurodevelopmental disorders such as ASD.

386 In addition to the above discussed metabolites, the untargeted analysis detected a large
387 number of compounds whose amounts in the culture were significantly altered by DEHP in a
388 dose-dependent fashion. Only a small fraction (79/1937) of these compounds could be assigned a
389 putative identity, as many of the detected features' MS/MS spectra could not be matched to
390 available databases for putative identification and subsequent confirmation. The total annotation
391 rate (204/5408) achieved in the present study is comparable to previous metabolomics studies on
392 the gut microbiota, which report annotation rates ranging from 2 (53) to 5% (54). Metabolite
393 identification clearly remains a bottleneck in untargeted metabolomics, and further efforts are
394 warranted to expand coverage of metabolites from commensal gut bacteria in spectral libraries.

395 The findings of the present study provide evidence that significant alterations could occur
396 even in developed microbiota in response to environmental chemical exposure, and that these
397 alterations include overproduction of selected bacterial metabolites. Several of these metabolites
398 have been found at elevated levels in urine or plasma of subjects diagnosed with
399 neurodevelopmental disorders, in particular ASD. Taken together with recent reports linking
400 phthalate exposure and ASD, our findings suggest the intriguing possibility that the chemical
401 could selectively modify the intestinal microbiota to promote the production of potentially toxic
402 metabolites such as *p*-cresol. Whether metabolites such as *p*-cresol casually contribute to
403 neurodevelopmental disorders or merely indicate dysbiosis associated with these disorders
404 remains to be elucidated. Further work is warranted to determine whether earlier (e.g.,

405 immediately after birth) and longer term DEHP exposure would lead to more severe dysbiosis
406 and affect behavioral outcomes.

407

408 **Materials and Methods**

409 **Materials** - All chemicals were purchased from Sigma Aldrich (St. Louis, MO) unless otherwise
410 specified. DEHP and MEHP were purchased from AccuStandard (New Haven, CT).

411

412 **DEHP exposure in mice** - Female C57BL/6J mice aged 4-5 weeks were purchased from Jackson
413 Laboratories (Bar Harbor, ME) and maintained on an *ad libitum* chow diet (8604 Teklad Rodent
414 diet, Envigo, Madison, WI). Mice were acclimatized to the animal facility for one week, and
415 were then given either vehicle (corn oil) or a low or high dose of DEHP (1 or 10 mg/kg
416 bodyweight/day) via oral gavage. Mice were gavaged with DEHP every other day. Fecal pellets
417 were collected immediately before the first gavage (day 0) and on days 7 and 14, flash frozen in
418 liquid nitrogen, and stored at -80°C. On day 14, animals were euthanized using asphyxiation
419 with CO₂. Animals were handled in accordance with the Texas A&M University Health Sciences
420 Center Institutional Animal Care and Use Committee guidelines under an approved animal use
421 protocol (AUP IACUC 2017-0145).

422

423 **In vitro culture of cecal luminal contents** – Whole cecum from female C57BL/6J mice (6-8
424 weeks of age) were harvested and transported to an anaerobic chamber (Coy Lab, Grass Lake,
425 MI) in an anaerobic transport medium (Anaerobe Systems, Morgan Hill, CA). Luminal contents
426 were isolated from the cecum inside the chamber, and then suspended into a slurry in 1 ml of
427 pre-reduced PBS containing 0.1% cysteine by vortexing the suspension for 2 min. Gut
428 microbiota medium (GMM) was prepared as described previously (27). Each batch of cecal

429 luminal contents slurry from a mouse was inoculated into a separate glass test tube containing 10
430 ml of GMM or GMM supplemented with a low or high dose of DEHP (10 or 100 μ M). The
431 inoculated tubes were incubated at 37°C for up to seven days under anaerobic conditions. Tubes
432 containing GMM but without inoculation and incubated under the same conditions were used as
433 negative controls. Culture (or medium) samples were collected on days 1 and 7 post inoculation
434 by removing test tubes from the incubator and centrifuging at 13,000g for 10 min at 4°C. The
435 cell pellet and supernatant were stored at -80°C for further analysis.

436

437 ***Extraction of metabolites*** – The fecal pellets and *in vitro* cecal luminal culture samples were
438 homogenized using lysing matrix E beads (MO BIO, Carlsbad, CA) on a bead beater (VWR,
439 Radnor, PA) with equal volume of cold methanol and half volume of chloroform. The samples
440 were homogenized for one min on the bead beater, cooled on ice for one minute, and
441 homogenized again for another 2 min. The samples were then centrifuged at 10,000g at 4 °C for
442 10 min. The supernatant was filtered through a 70- μ m sterile nylon cell strainer into a clean
443 sample tube and mixed with 0.6 ml of ice-cold water using a vortex mixer. This mixture was
444 centrifuged again at 10,000g for 5 min to obtain phase separation. The upper and lower phase
445 were separately collected using a syringe while taking care not to disturb the interface. The upper
446 phase was dried to a pellet using a vacufuge (Eppendorf, Hauppauge, NY), and stored at -80 °C
447 until further analysis. Prior to LC-MS analysis, the dried samples were reconstituted in 50 μ l of
448 methanol/water (1:1, v/v).

449

450 ***Untargeted metabolomics*** – The extracted samples were analyzed for global metabolite profiles
451 using information-dependent acquisition (IDA) experiments performed on a triple-quadrupole
452 time-of-flight instrument (5600+, AB Sciex) coupled to a binary pump HPLC system (1260

453 Infinity, Agilent). Each sample was analyzed twice, using two different combinations of LC
454 methods and ionization modes to obtain broad coverage of metabolites having varying polarities
455 and isoelectric points (see Supplementary Methods). Raw data were processed in MarkerView
456 (v. 1.2, AB Sciex) to determine the ion peaks. The peaks were aligned based on m/z and
457 retention time (RT), (30 ppm and 2.5 min tolerance, respectively), and then filtered based on
458 intensity (100 cps threshold) to eliminate low quality peaks. An additional filter was applied to
459 retain only monoisotopic ions. The retained ions were organized into a feature table, with each
460 feature specified by m/z and RT. In the case a precursor ion detected by the TOF survey scan
461 triggered an MS/MS scan, the corresponding MS/MS spectrum was extracted from the product
462 ion scan data and added to the feature table. Each feature was searched against spectral libraries
463 in METLIN (55), HMDB (56), and NIST (57). The MS/MS spectrum of each feature was also
464 analyzed using *in silico* fragmentation tools MetFrag (58) and CFM-ID (59). These analyses
465 identified several annotations for many of the features. To systematically determine the most
466 likely identities for these features in the context of murine cecal microbiota metabolism, we
467 applied an automated annotation procedure ('BioCAN') that combines the outputs from the
468 database searches and fragmentation analyses with a metabolic model (see below) for the
469 biological system of interest (60). Briefly, BioCAN maps each unique mass in the feature table
470 onto a metabolic network representing the enzymatic reactions possible in the system of interest,
471 and evaluates the likelihood a correct mapping between a detected mass and a metabolite in the
472 network has occurred based on how many other metabolites in the neighborhood of the
473 metabolite in question also map to a detected mass. Features annotated with high confidence
474 were further inspected manually and confirmed by matching the product ion spectrum to
475 standards in the aforementioned reference databases. In cases where no reference MS/MS spectra
476 were available, a pure standard was run to confirm the metabolite identity. Relative amounts of

477 metabolites were quantified using MultiQuant 2.1 (AB Sciex) by manually integrating the
478 corresponding peak areas in the extracted ion chromatograms (XICs).

479

480 **Targeted analysis of MEHP** - The fate of DEHP in the cecal culture was characterized by
481 quantifying the amount of its major metabolic product, MEHP. Targeted analysis of MEHP
482 utilized a product ion scan experiment as described previously (61).

483

484 **16S rRNA sequencing analysis** – Fecal and *in vitro* cecal luminal culture pellets were
485 homogenized and microbial DNA was extracted from the homogenate using the standard
486 protocol for Power soil DNA extraction kit (MO BIO). The V4 region of 16S rRNA was
487 sequenced on a MiSeq Illumina platform using protocols for paired-end sequencing from
488 Kozhich et al. (2013) at the Microbial Analysis, Resources, and Services (MARS) core facility at
489 the University of Connecticut. Sequence reads were quality filtered, denoised, joined, chimera
490 filtered, aligned and classified using QIIME (62, 63). The SILVA database (28) was used for
491 alignment and classification (97% similarity) of the OTUs. The OTU counts were normalized by
492 subsampling to the lowest number of OTUs found in the sample.

493

494 **Metabolic model** – The OTU tables from QIIME analysis were used to build a metabolic model
495 linking bacterial groups detected in the cecal cultures to metabolites that can be produced by
496 these groups. To select species for inclusion in the model, we tabulated the most abundant OTUs
497 detected in all samples from both days 1 and 7 of GMM culture, with a 0.01% cutoff for relative
498 abundance. The genera associated with these OTUs were searched against the KEGG Organisms
499 database to compile a list of organisms that have a complete genome sequence and an assigned
500 KEGG organism code (64). This list was then manually curated to remove species unlikely to be

501 present in murine cecum (e.g., soil dwelling bacteria and extremophiles) by searching a
502 microbiome database (65) and carefully examining the published literature. From this curated
503 list, we generated a matrix linking an organism to reactions encoded by its genome. First, the
504 KEGG Orthology identifiers (K numbers) and Enzyme Commission (EC) numbers associated
505 with the organism codes were collected using the KEGG REST API. These K and EC numbers
506 were then linked to KEGG reaction identifiers (R numbers). The linkages between organism
507 codes and R numbers were arranged into an organism-reaction (**OR_{KEGG}**) matrix, where each
508 element (i, j) denotes the presence ('1') or absence ('0') of a reaction i in organism j .

509 The organisms in **OR_{KEGG}** accounted for 48 of the 119 most abundant genera in the cecal
510 cultures. The remaining 71 genera were searched against the UniProt database to determine if
511 high-quality genome sequences with functional annotation were available for any of the member
512 strains. After removing species that are unlikely present in the murine cecum, organisms with
513 high-quality functional annotations were added to an organism-enzyme matrix (**OE_{UniProt}**), where
514 each element (i, j) denotes the presence ('1') or absence ('0') of an enzyme i in organism
515 j . The amino acid sequences from each of the remaining organisms lacking annotated genomes
516 were downloaded from GenBank and assigned K numbers using BlastKOALA (66). The
517 resulting linkages between organisms and K numbers were arranged into an organism-orthology
518 matrix (**OK_{UniProt}**). The K and EC numbers of these two matrices were linked to R numbers to
519 generate a second organism-reaction matrix (**OR_{UniProt}**). The two matrices **OR_{KEGG}** and
520 **OR_{UniProt}** were combined to produce a final organism-reaction matrix (**OR**) for all detected
521 genera with member species that have high-quality genome sequences. The metabolites
522 associated with each organism were found by linking the reactions with their primary substrate-
523 product pairs as defined by KEGG's RCLASS data.

524

525 **Statistical analysis** –OTUs observed only once across all samples were filtered prior to PCA and
526 PLS-DA in MATLAB (v. R2018a). Linear discriminant analysis of the effect size (LEfSe) was
527 used to characterize differences in the OTU counts between samples (67). Effects were
528 considered statistically significant if they were assigned a q-value less than 0.05. A two-tailed t-
529 test with a cutoff *p*-value of 0.05 was used to test for statistical significance of differences in
530 metabolite levels between treatment groups. Pearson correlation coefficients (PCCs) were
531 calculated between OTU counts (relative abundance) and peak areas of metabolites. Statistical
532 significance of the PCCs was determined based on p-values calculated using a two-tailed *t*-test,
533 and corrected for false-discovery rate using the Benjamini-Hochberg (B-H) method (68).
534 Statistically significant correlations (B-H adjusted *p*-value < 0.05) between OTUs (at the level of
535 genus) and metabolites were visualized in Cytoscape (v. 3.0).

536

537 **Acknowledgments**

538 This work was supported by grants from the NSF (1264502) and NIGMS (GM106251) to KL
539 and AJ, the Nesbitt Chair to AJ, and grants from NSF (1337760) and NCI (CA211839) to KL.

540

541 **Author Contributions**

542 S.M., R.M., K.L., and A.J. designed the study. M.L., R.M., S.M., C.H., and R.C.A. performed
543 the experiments. M.L., R.M., and N.A. analyzed the data. M.L., R.M., K.L., and A.J. wrote the
544 manuscript.

545 ¹M.L. and R.M. contributed equally to this work.

546

547 **Competing Interests**

548 The authors declare no competing interests.

549 **References**

- 550 1. Tamboli C, Neut C, Desreumaux P, Colombel J. 2004. Dysbiosis in inflammatory bowel
551 disease. *Gut* 53:1-4.
- 552 2. Sobhani I, Tap J, Roudot-Thoraval F, Roperch JP, Letulle S, Langella P, Corthier G, Van
553 Nhieu JT, Furet JP. 2011. Microbial dysbiosis in colorectal cancer (CRC) patients. *PloS*
554 *one* 6:e16393.
- 555 3. Hoyles L, Fernandez-Real JM, Federici M, Serino M, Abbott J, Charpentier J, Heymes C,
556 Luque JL, Anthony E, Barton RH, Chilloux J, Myridakis A, Martinez-Gili L, Moreno-
557 Navarrete JM, Benhamed F, Azalbert V, Blasco-Baque V, Puig J, Xifra G, Ricart W,
558 Tomlinson C, Woodbridge M, Cardellini M, Davato F, Cardolini I, Porzio O, Gentileschi
559 P, Lopez F, Foufelle F, Butcher SA, Holmes E, Nicholson JK, Postic C, Burcelin R,
560 Dumas ME. 2018. Molecular phenomics and metagenomics of hepatic steatosis in non-
561 diabetic obese women. *Nat Med* 24:1070-1080.
- 562 4. Qin J, Li Y, Cai Z, Li S, Zhu J, Zhang F, Liang S, Zhang W, Guan Y, Shen D. 2012. A
563 metagenome-wide association study of gut microbiota in type 2 diabetes. *Nature* 490:55.
- 564 5. Rogers G, Keating D, Young R, Wong M, Licinio J, Wesselingh S. 2016. From gut
565 dysbiosis to altered brain function and mental illness: mechanisms and pathways.
566 *Molecular psychiatry* 21:738.
- 567 6. Rosenfeld CS. 2017. Gut Dysbiosis in Animals Due to Environmental Chemical
568 Exposures. *Frontiers in cellular and infection microbiology* 7:396-396.
- 569 7. Erythropel HC, Maric M, Nicell JA, Leask RL, Yargeau V. 2014. Leaching of the
570 plasticizer di(2-ethylhexyl)phthalate (DEHP) from plastic containers and the question of
571 human exposure. *Appl Microbiol Biotechnol* 98:9967-81.

- 572 8. Kay VR, Chambers C, Foster WG. 2013. Reproductive and developmental effects of
573 phthalate diesters in females. *Critical reviews in toxicology* 43:200-219.
- 574 9. Kardas F, Bayram AK, Demirci E, Akin L, Ozmen S, Kendirci M, Canpolat M, Oztop
575 DB, Narin F, Gumus H, Kumandas S, Per H. 2016. Increased Serum Phthalates (MEHP,
576 DEHP) and Bisphenol A Concentrations in Children With Autism Spectrum Disorder:
577 The Role of Endocrine Disruptors in Autism Etiopathogenesis. *J Child Neurol* 31:629-35.
- 578 10. Kang DW, Ilhan ZE, Isern NG, Hoyt DW, Howsmon DP, Shaffer M, Lozupone CA,
579 Hahn J, Adams JB, Krajmalnik-Brown R. 2018. Differences in fecal microbial
580 metabolites and microbiota of children with autism spectrum disorders. *Anaerobe*
581 49:121-131.
- 582 11. Ribiere C, Peyret P, Parisot N, Darcha C, Dechelotte PJ, Barnich N, Peyretailade E,
583 Boucher D. 2016. Oral exposure to environmental pollutant benzo[a]pyrene impacts the
584 intestinal epithelium and induces gut microbial shifts in murine model. *Sci Rep* 6:31027.
- 585 12. DeLuca JA, Allred KF, Menon R, Riordan R, Weeks BR, Jayaraman A, Allred CD. 2018.
586 Bisphenol-A alters microbiota metabolites derived from aromatic amino acids and
587 worsens disease activity during colitis. *Exp Biol Med (Maywood)* 243:864-875.
- 588 13. Hsiao EY, McBride SW, Hsien S, Sharon G, Hyde ER, McCue T, Codelli JA, Chow J,
589 Reisman SE, Petrosino JF. 2013. Microbiota modulate behavioral and physiological
590 abnormalities associated with neurodevelopmental disorders. *Cell* 155:1451-1463.
- 591 14. West PR, Amaral DG, Bais P, Smith AM, Egnash LA, Ross ME, Palmer JA, Fontaine
592 BR, Conard KR, Corbett BA, Cezar GG, Donley EL, Burrier RE. 2014. Metabolomics as
593 a tool for discovery of biomarkers of autism spectrum disorder in the blood plasma of
594 children. *PLoS One* 9:e112445.

- 595 15. Dieme B, Mavel S, Blasco H, Tripi G, Bonnet-Brilhault F, Malvy J, Bocca C, Andres
596 CR, Nadal-Desbarats L, Emond P. 2015. Metabolomics Study of Urine in Autism
597 Spectrum Disorders Using a Multiplatform Analytical Methodology. *J Proteome Res*
598 14:5273-82.
- 599 16. Hannon PR, Niermann S, Flaws JA. 2016. Acute Exposure to Di(2-Ethylhexyl) Phthalate
600 in Adulthood Causes Adverse Reproductive Outcomes Later in Life and Accelerates
601 Reproductive Aging in Female Mice. *Toxicol Sci* 150:97-108.
- 602 17. Kloting N, Hesselbarth N, Gericke M, Kunath A, Biemann R, Chakaroun R, Kosacka J,
603 Kovacs P, Kern M, Stumvoll M, Fischer B, Rolle-Kampczyk U, Feltens R, Otto W,
604 Wissenbach DK, von Bergen M, Bluher M. 2015. Di-(2-Ethylhexyl)-Phthalate (DEHP)
605 Causes Impaired Adipocyte Function and Alters Serum Metabolites. *PLoS One*
606 10:e0143190.
- 607 18. Holahan MR, Smith CA, Luu BE, Storey KB. 2018. Preadolescent Phthalate (DEHP)
608 Exposure Is Associated With Elevated Locomotor Activity and Reward-Related Behavior
609 and a Reduced Number of Tyrosine Hydroxylase Positive Neurons in Post-Adolescent
610 Male and Female Rats. *Toxicol Sci* 165:512-530.
- 611 19. Leclercq S, Mian FM, Stanisiz AM, Bindels LB, Cambier E, Ben-Amram H, Koren O,
612 Forsythe P, Bienenstock J. 2017. Low-dose penicillin in early life induces long-term
613 changes in murine gut microbiota, brain cytokines and behavior. *Nat Commun* 8:15062.
- 614 20. Joly Condet C, Bach V, Mayeur C, Gay-Queheillard J, Khorsi-Cauet H. 2015.
615 Chlorpyrifos Exposure During Perinatal Period Affects Intestinal Microbiota Associated
616 With Delay of Maturation of Digestive Tract in Rats. *J Pediatr Gastroenterol Nutr* 61:30-
617 40.

- 618 21. Reddivari L, Veeramachaneni DNR, Walters WA, Lozupone C, Palmer J, Hewage MKK,
619 Bhatnagar R, Amir A, Kennett MJ, Knight R, Vanamala JKP. 2017. Perinatal Bisphenol
620 A Exposure Induces Chronic Inflammation in Rabbit Offspring via Modulation of Gut
621 Bacteria and Their Metabolites. *mSystems* 2.
- 622 22. Hu J, Raikhel V, Gopalakrishnan K, Fernandez-Hernandez H, Lambertini L, Manservigi
623 F, Falcioni L, Bua L, Belpoggi F, S LT, Chen J. 2016. Effect of postnatal low-dose
624 exposure to environmental chemicals on the gut microbiome in a rodent model.
625 *Microbiome* 4:26.
- 626 23. Spor A, Koren O, Ley R. 2011. Unravelling the effects of the environment and host
627 genotype on the gut microbiome. *Nat Rev Microbiol* 9:279-90.
- 628 24. Zhang L, Nichols RG, Correll J, Murray IA, Tanaka N, Smith PB, Hubbard TD,
629 Sebastian A, Albert I, Hatzakis E, Gonzalez FJ, Perdew GH, Patterson AD. 2015.
630 Persistent Organic Pollutants Modify Gut Microbiota-Host Metabolic Homeostasis in
631 Mice Through Aryl Hydrocarbon Receptor Activation. *Environ Health Perspect* 123:679-
632 88.
- 633 25. Zhang LS, Davies SS. 2016. Microbial metabolism of dietary components to bioactive
634 metabolites: opportunities for new therapeutic interventions. *Genome Med* 8:46.
- 635 26. Tomita I, Nakamura Y, Yagi Y, Tutikawa K. 1986. Fetotoxic effects of mono-2-
636 ethylhexyl phthalate (MEHP) in mice. *Environ Health Perspect* 65:249-54.
- 637 27. Goodman AL, Kallstrom G, Faith JJ, Reyes A, Moore A, Dantas G, Gordon JI. 2011.
638 Extensive personal human gut microbiota culture collections characterized and
639 manipulated in gnotobiotic mice. *Proc Natl Acad Sci U S A* 108:6252-7.

- 640 28. Quast C, Pruesse E, Yilmaz P, Gerken J, Schweer T, Yarza P, Peplies J, Glockner FO.
641 2013. The SILVA ribosomal RNA gene database project: improved data processing and
642 web-based tools. *Nucleic Acids Res* 41:D590-6.
- 643 29. Asshauer KP, Wemheuer B, Daniel R, Meinicke P. 2015. Tax4Fun: predicting functional
644 profiles from metagenomic 16S rRNA data. *Bioinformatics* 31:2882-4.
- 645 30. Javurek AB, Spollen WG, Johnson SA, Bivens NJ, Bromert KH, Givan SA, Rosenfeld
646 CS. 2016. Effects of exposure to bisphenol A and ethinyl estradiol on the gut microbiota
647 of parents and their offspring in a rodent model. *Gut Microbes* 7:471-485.
- 648 31. Wu J, Wen XW, Faulk C, Boehnke K, Zhang H, Dolinoy DC, Xi C. 2016. Perinatal Lead
649 Exposure Alters Gut Microbiota Composition and Results in Sex-specific Bodyweight
650 Increases in Adult Mice. *Toxicol Sci* 151:324-33.
- 651 32. Song Y, Liu C, Finegold SM. 2004. Real-time PCR quantitation of clostridia in feces of
652 autistic children. *Appl Environ Microbiol* 70:6459-65.
- 653 33. Luna RA, Oezguen N, Balderas M, Venkatachalam A, Runge JK, Versalovic J, Veenstra-
654 VanderWeele J, Anderson GM, Savidge T, Williams KC. 2017. Distinct Microbiome-
655 Neuroimmune Signatures Correlate With Functional Abdominal Pain in Children With
656 Autism Spectrum Disorder. *Cell Mol Gastroenterol Hepatol* 3:218-230.
- 657 34. Van de Wiele T, Van den Abbeele P, Ossieur W, Possemiers S, Marzorati M. 2015. The
658 Simulator of the Human Intestinal Microbial Ecosystem (SHIME((R))), p 305-317. *In*
659 Verhoeckx K, Cotter P, Lopez-Exposito I, Kleiveland C, Lea T, Mackie A, Requena T,
660 Swiatecka D, Wichers H (ed), *The Impact of Food Bioactives on Health: in vitro and ex*
661 *vivo models* doi:10.1007/978-3-319-16104-4_27, Cham (CH).
- 662 35. Marcobal A, De las Rivas B, Landete JM, Tabera L, Munoz R. 2012. Tyramine and
663 phenylethylamine biosynthesis by food bacteria. *Crit Rev Food Sci Nutr* 52:448-67.

- 664 36. Ramezani A, Massy ZA, Meijers B, Evenepoel P, Vanholder R, Raj DS. 2016. Role of
665 the Gut Microbiome in Uremia: A Potential Therapeutic Target. *Am J Kidney Dis*
666 67:483-98.
- 667 37. Shaw W. 2010. Increased urinary excretion of a 3-(3-hydroxyphenyl)-3-
668 hydroxypropionic acid (HPHPA), an abnormal phenylalanine metabolite of *Clostridia*
669 spp. in the gastrointestinal tract, in urine samples from patients with autism and
670 schizophrenia. *Nutr Neurosci* 13:135-43.
- 671 38. Duncan SH, Louis P, Flint HJ. 2004. Lactate-utilizing bacteria, isolated from human
672 feces, that produce butyrate as a major fermentation product. *Appl Environ Microbiol*
673 70:5810-7.
- 674 39. LeBlanc JG, Milani C, de Giori GS, Sesma F, van Sinderen D, Ventura M. 2013. Bacteria
675 as vitamin suppliers to their host: a gut microbiota perspective. *Current opinion in*
676 *biotechnology* 24:160-168.
- 677 40. Liu R, Li Q, Ma R, Lin X, Xu H, Bi K. 2013. Determination of polyamine metabolome in
678 plasma and urine by ultrahigh performance liquid chromatography-tandem mass
679 spectrometry method: application to identify potential markers for human hepatic cancer.
680 *Anal Chim Acta* 791:36-45.
- 681 41. Dawson LF, Donahue EH, Cartman ST, Barton RH, Bundy J, McNerney R, Minton NP,
682 Wren BW. 2011. The analysis of para-cresol production and tolerance in *Clostridium*
683 *difficile* 027 and 012 strains. *BMC Microbiol* 11:86.
- 684 42. Moss CW, Hatheway CL, Lambert MA, McCroskey LM. 1980. Production of
685 phenylacetic and hydroxyphenylacetic acids by *clostridium botulinum* type G. *J Clin*
686 *Microbiol* 11:743-5.

- 687 43. Hwang N, Eom T, Gupta SK, Jeong SY, Jeong DY, Kim YS, Lee JH, Sadowsky MJ,
688 Unno T. 2017. Genes and Gut Bacteria Involved in Luminal Butyrate Reduction Caused
689 by Diet and Loperamide. *Genes (Basel)* 8.
- 690 44. Gillam EM, Notley LM, Cai H, De Voss JJ, Guengerich FP. 2000. Oxidation of indole by
691 cytochrome P450 enzymes. *Biochemistry* 39:13817-24.
- 692 45. Ma Q, Zhang X, Qu Y. 2018. Biodegradation and Biotransformation of Indole: Advances
693 and Perspectives. *Front Microbiol* 9:2625.
- 694 46. Madsen EL, Bollag JM. 1989. Pathway of Indole Metabolism by a Denitrifying
695 Microbial Community. *Archives of Microbiology* 151:71-76.
- 696 47. Claus SP, Guillou H, Ellero-Simatos S. 2016. The gut microbiota: a major player in the
697 toxicity of environmental pollutants? *Npj Biofilms And Microbiomes* 2:16003.
- 698 48. De Angelis M, Piccolo M, Vannini L, Siragusa S, De Giacomo A, Serrazanetti DI,
699 Cristofori F, Guerzoni ME, Gobbetti M, Francavilla R. 2013. Fecal microbiota and
700 metabolome of children with autism and pervasive developmental disorder not otherwise
701 specified. *PLoS One* 8:e76993.
- 702 49. Gabriele S, Sacco R, Cerullo S, Neri C, Urbani A, Tripi G, Malvy J, Barthelemy C,
703 Bonnet-Brihault F, Persico AM. 2014. Urinary p-cresol is elevated in young French
704 children with autism spectrum disorder: a replication study. *Biomarkers* 19:463-70.
- 705 50. Bourassa MW, Alim I, Bultman SJ, Ratan RR. 2016. Butyrate, neuroepigenetics and the
706 gut microbiome: Can a high fiber diet improve brain health? *Neurosci Lett* 625:56-63.
- 707 51. Selmer T, Andrei PI. 2001. p-Hydroxyphenylacetate decarboxylase from *Clostridium*
708 *difficile*. A novel glyceryl radical enzyme catalysing the formation of p-cresol. *Eur J*
709 *Biochem* 268:1363-72.

- 710 52. Jaglin M, Rhimi M, Philippe C, Pons N, Bruneau A, Goustard B, Dauge V, Maguin E,
711 Naudon L, Rabot S. 2018. Indole, a Signaling Molecule Produced by the Gut Microbiota,
712 Negatively Impacts Emotional Behaviors in Rats. *Front Neurosci* 12:216.
- 713 53. Fujisaka S, Avila-Pacheco J, Soto M, Kostic A, Dreyfuss JM, Pan H, Ussar S, Altindis E,
714 Li N, Bry L, Clish CB, Kahn CR. 2018. Diet, Genetics, and the Gut Microbiome Drive
715 Dynamic Changes in Plasma Metabolites. *Cell Rep* 22:3072-3086.
- 716 54. Franzosa EA, Sirota-Madi A, Avila-Pacheco J, Fornelos N, Haiser HJ, Reinker S,
717 Vatanen T, Hall AB, Mallick H, McIver LJ, Sauk JS, Wilson RG, Stevens BW, Scott JM,
718 Pierce K, Deik AA, Bullock K, Imhann F, Porter JA, Zhernakova A, Fu J, Weersma RK,
719 Wijmenga C, Clish CB, Vlamakis H, Huttenhower C, Xavier RJ. 2019. Gut microbiome
720 structure and metabolic activity in inflammatory bowel disease. *Nat Microbiol* 4:293-305.
- 721 55. Smith CA, O'Maille G, Want EJ, Qin C, Trauger SA, Brandon TR, Custodio DE,
722 Abagyan R, Siuzdak G. 2005. METLIN: a metabolite mass spectral database. *Ther Drug*
723 *Monit* 27:747-51.
- 724 56. Wishart DS, Tzur D, Knox C, Eisner R, Guo AC, Young N, Cheng D, Jewell K, Arndt D,
725 Sawhney S, Fung C, Nikolai L, Lewis M, Coutouly MA, Forsythe I, Tang P, Shrivastava
726 S, Jeroncic K, Stothard P, Amegbey G, Block D, Hau DD, Wagner J, Miniaci J, Clements
727 M, Gebremedhin M, Guo N, Zhang Y, Duggan GE, Macinnis GD, Weljie AM,
728 Dowlatabadi R, Bamforth F, Clive D, Greiner R, Li L, Marrie T, Sykes BD, Vogel HJ,
729 Querengesser L. 2007. HMDB: the Human Metabolome Database. *Nucleic Acids Res*
730 35:D521-6.
- 731 57. Johnson S. 2018. NIST Standard Reference Database 1A v17. National Institute of
732 Standards and Technology,

- 733 58. Wolf S, Schmidt S, Muller-Hannemann M, Neumann S. 2010. In silico fragmentation for
734 computer assisted identification of metabolite mass spectra. *BMC Bioinformatics* 11:148.
- 735 59. Allen F, Pon A, Wilson M, Greiner R, Wishart D. 2014. CFM-ID: a web server for
736 annotation, spectrum prediction and metabolite identification from tandem mass spectra.
737 *Nucleic Acids Res* 42:W94-9.
- 738 60. Alden N, Krishnan S, Porokhin V, Raju R, McElearney K, Gilbert A, Lee K. 2017.
739 Biologically Consistent Annotation of Metabolomics Data. *Anal Chem* 89:13097-13104.
- 740 61. Manteiga S, Lee K. 2017. Monoethylhexyl Phthalate Elicits an Inflammatory Response in
741 Adipocytes Characterized by Alterations in Lipid and Cytokine Pathways. *Environ*
742 *Health Perspect* 125:615-622.
- 743 62. Edgar RC, Haas BJ, Clemente JC, Quince C, Knight R. 2011. UCHIME improves
744 sensitivity and speed of chimera detection. *Bioinformatics* 27:2194-200.
- 745 63. Caporaso JG, Kuczynski J, Stombaugh J, Bittinger K, Bushman FD, Costello EK, Fierer
746 N, Pena AG, Goodrich JK, Gordon JI, Huttley GA, Kelley ST, Knights D, Koenig JE,
747 Ley RE, Lozupone CA, McDonald D, Muegge BD, Pirrung M, Reeder J, Sevinsky JR,
748 Turnbaugh PJ, Walters WA, Widmann J, Yatsunenko T, Zaneveld J, Knight R. 2010.
749 QIIME allows analysis of high-throughput community sequencing data. *Nat Methods*
750 7:335-6.
- 751 64. Kanehisa M, Goto S. 2000. KEGG: kyoto encyclopedia of genes and genomes. *Nucleic*
752 *Acids Res* 28:27-30.
- 753 65. Lloyd-Price J, Mahurkar A, Rahnavard G, Crabtree J, Orvis J, Hall AB, Brady A, Creasy
754 HH, McCracken C, Giglio MG, McDonald D, Franzosa EA, Knight R, White O,
755 Huttenhower C. 2017. Strains, functions and dynamics in the expanded Human
756 Microbiome Project. *Nature* 550:61-66.

- 757 66. Kanehisa M, Sato Y, Morishima K. 2016. BlastKOALA and GhostKOALA: KEGG
758 Tools for Functional Characterization of Genome and Metagenome Sequences. *J Mol*
759 *Biol* 428:726-731.
- 760 67. Segata N, Izard J, Waldron L, Gevers D, Miropolsky L, Garrett WS, Huttenhower C.
761 2011. Metagenomic biomarker discovery and explanation. *Genome biology* 12:R60.
- 762 68. Benjamini Y, Hochberg Y. 1995. Controlling the False Discovery Rate: A Practical and
763 Powerful Approach to Multiple Testing. *Journal of the Royal Statistical Society Series B*
764 (Methodological) 57:289-300.
- 765

766 **Figure Legends**

767 Figure 1. Metagenomic (16S rRNA) analysis of fecal microbiota from DEHP-exposed mice. (A)
768 PCA on OTU counts. The percentage represents the percent variance explained by each axis. (B)
769 Alpha diversity and (C) LefSE analysis of fecal microbiota OTU counts.

770

771 Figure 2. Metabolite analysis of fecal microbiota from DEHP-exposed mice. (A) LC-MS
772 identification of MEHP in fecal material collected at day 7 and 14 from animals fed a low (+) or
773 high dose (++) of DEHP. The level of MEHP in control samples (-) was below the limit of
774 detection. (B) Scatter plot of the first two PC scores from PCA of the metabolite data.

775

776 Figure 3. Metagenomic analysis of *in vitro* cecal luminal contents culture. (A) Phylum-level
777 classification of unique OTUs in DEHP-treated cultures. (B) Relative abundance of bacterial
778 genera on day 1 and 7 in control (GMM) and DEHP-treated cultures.

779

780 Figure 4. Metabolite profiles from *in vitro* cultured cecal luminal contents. (A) Scatter plot of the
781 first two scores from PCA representing microbial metabolites produced on day 1 and day 7. (B)
782 Heat map of detected ion peaks with different patterns of substrate utilization and product
783 formation. (C) Percentage distribution of detected features classified as products, substrates, or
784 intermediates based on their time profiles. (D) Profiles of tryptophan and indole in the cecal
785 luminal content cultures. Filled and open markers represent inoculated cultures and tubes
786 incubated without luminal contents, respectively. Triangles and circles represent day 1 and 7
787 time points, respectively. The colors correspond to the classifications in the heat map and pie
788 chart. *: p -value<0.05 when compared to inoculated culture at day 1 (two-tailed t-test).

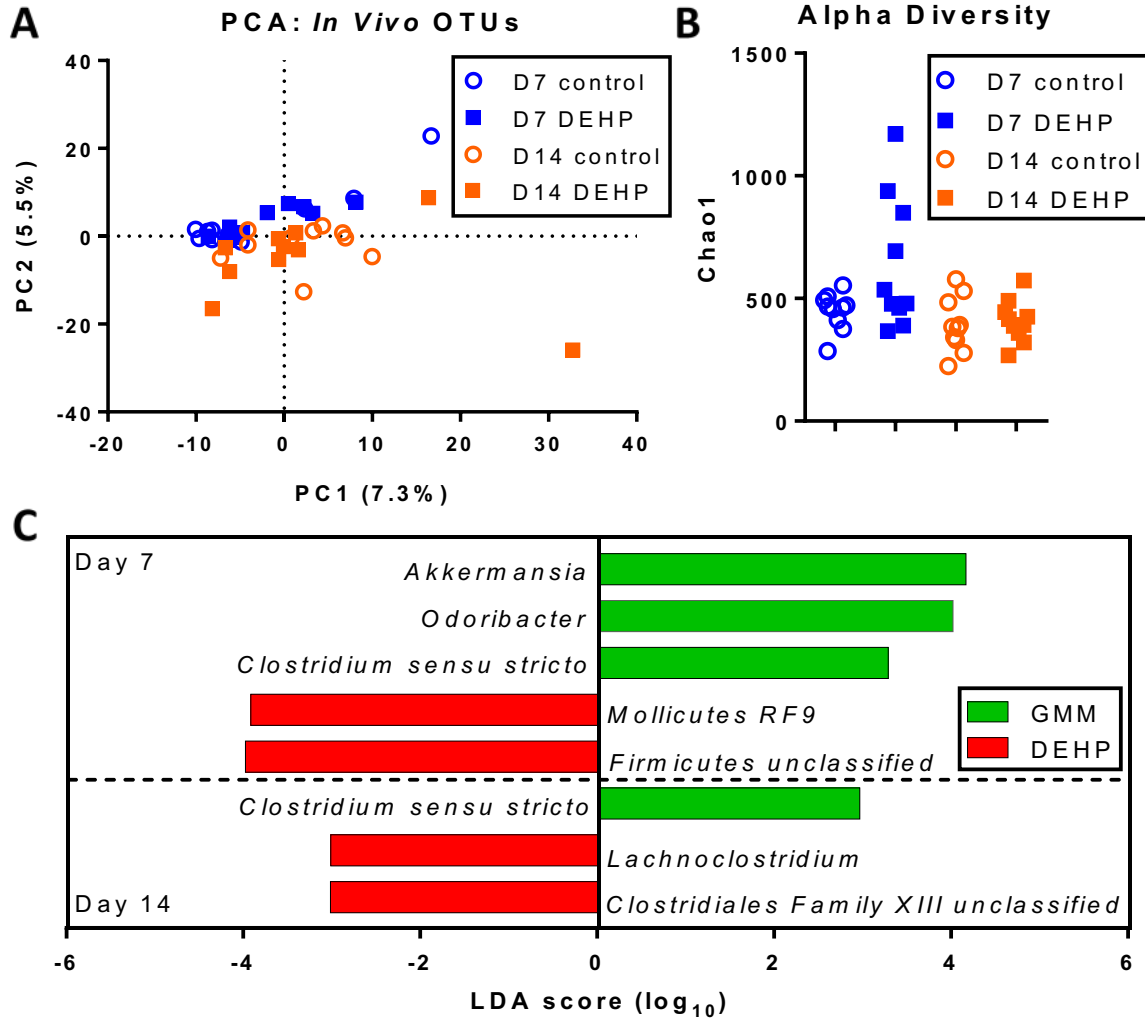
789

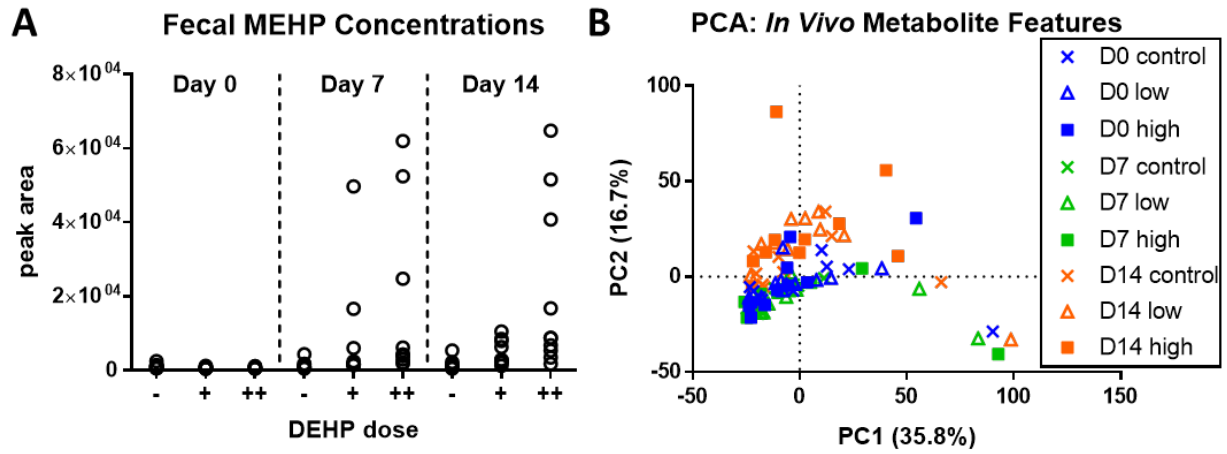
790 Figure 5. Model of metabolic reactions in *in vitro* culture of cecal luminal contents. (A) Fraction
791 of genus-level OTU counts represented by the metabolic model. (B) Hierarchical clustering of
792 genera and metabolites in the model. (C) Correlation network showing significant Pearson
793 correlations between genera (circles) and metabolites (squares). Fold-change from day 1 to 7 is
794 indicated by red (decrease) and green (increase) colors. Solid edges between nodes indicate that
795 the genus has at least one species capable of metabolizing the connected metabolite (per database
796 annotation of the genome), while dotted lines indicate a purely empirical correlation.

797

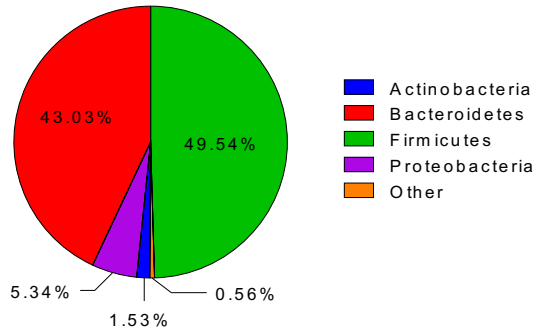
798 Figure 6. Significant microbial and metabolite changes in *in vitro* cultured cecal luminal contents
799 with DEHP. (A) LefSe analysis of genus-level microbiota changes induced by DEHP. (B)
800 Scatter plot of first two PC scores from PCA of metabolite features detected in the cecal cultures
801 (positive mode IDA data). (C) Dose-dependent changes in *p*-cresol and butyric acid with DEHP
802 on day 7. *: $-value < 0.05$ when compared to day 7 culture without DEHP addition (two-tailed t-
803 test).

Figures

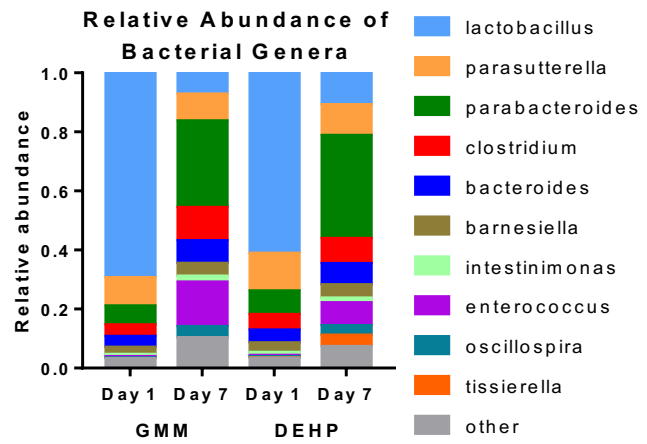




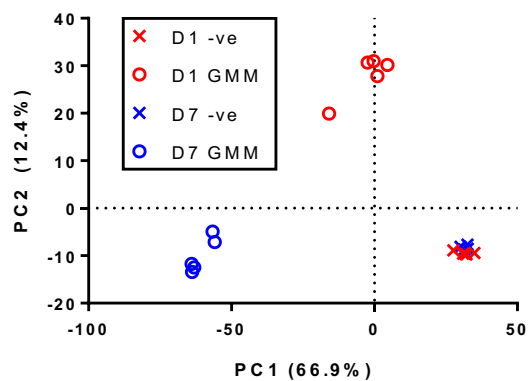
A Unique OTUs



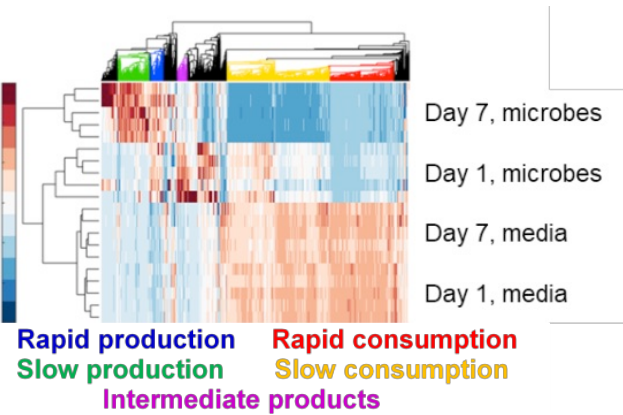
B



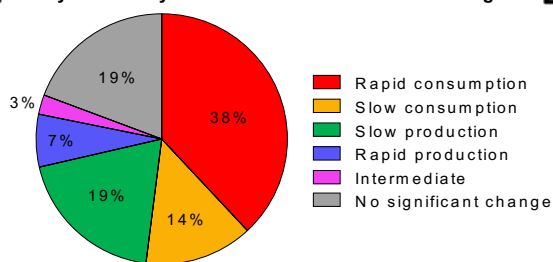
A PCA: *In Vitro* Metabolite Features



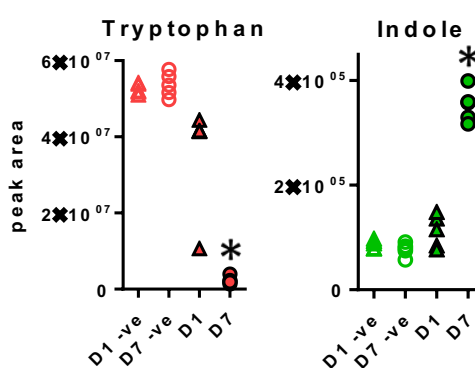
B



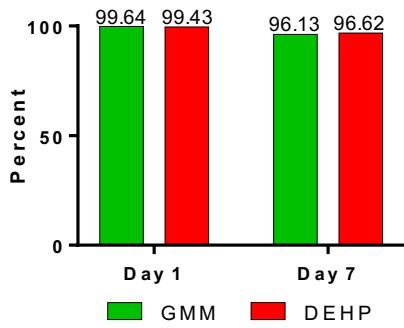
C Day 1 to Day 7 Metabolite Feature Changes



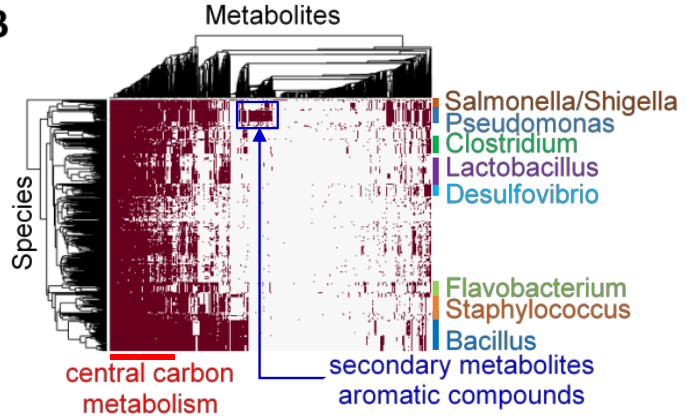
D



A OTU Counts Represented by Metabolic Model



B



C

